Available online at www.sciencedirect.com

ScienceDirect

Advances in Space Research 70 (2022) 1429–1440

ADVANCES IN SPACE RESEARCH (a COSPAR publication)

www.elsevier.com/locate/asr

Analysis of local geomagnetic index under the influence of equatorial electrojet (EEJ) at the equatorial Phuket geomagnetic station in Thailand

Lin M.M. Myint [a,*], Kornyanat Hozumi [b], Susumu Saito [c], Pornchai Supnithi [a]

[a] School of Engineering, King Mongkut's Institute of Technology Ladkrabang, Bangkok 10520, Thailand
[b] National Institute of Information and Communications Technology, Koganei, Tokyo 184-8795, Japan
[c] Electronic Navigation Research Institute, National Institute of Maritime, Port and Aviation Technology, Tokyo, 182-0012, Japan

Received 16 March 2022; received in revised form 7 June 2022; accepted 9 June 2022
Available online 17 June 2022

Abstract

The local K-index is an important proxy to monitor geomagnetic disturbances due to the solar wind in space weather study. The diurnal variation of geomagnetic fields observed in the magnetic equatorial region is dominated by the equatorial electrojet (EEJ), and the variation of EEJ is directly related to the local ionospheric dynamics; therefore, in this work, the local K-index is generated by based on the geomagnetic field measurement at an equatorial geomagnetic station in Phuket, Thailand and the effects of EEJ on the computed local K-indices are analyzed. At each station, an L9 (the lower limit for K = 9) value is set to develop a conversion table between the magnetic range scales and K-indices, and that L9 value must be assigned based on the characterization of the geomagnetic variations at that station. In this work, suitable L9 values are determined by analyzing the distributions of the local K-index and the planetary geomagnetic index, Kp-index. According to the results in the present study, the L9 value of 500 nT can provide local K-indices that can classify the geomagnetic disturbances more correctly. The results show that 40% of the local K-index is consistent with the Kp-index, and about 45% of the local K indices are ±1 deviated from Kp-indices. It is found that using the suitable L9 value can partially control the EEJ's dominance on K-index. Moreover, we investigated the seasonal and day-to-day variability of the diurnal variation of the geomagnetic fields from the Phuket station. Upon reviewing the data, the equatorial geomagnetic field variations were consistent with the planetary geomagnetic activity levels, and the day-to-day changes of the daytime field amplitudes were relatively high in the high solar activity year and moderate in the low solar activity year.

Keywords: Geomagnetic indices; Geomagnetic disturbances; Equatorial electrojet; local K-index; Kp-index, magnetic equator

1. Introduction

Monitoring geomagnetic disturbances is vital in space weather studies because severe disturbances or geomagnetic storms can result in service degradation of technologies, for example, satellite communication and navigation, electric power grid systems and high-frequency radio communications (Astafyeva et al., 2014; Baker et al., 2004; Lanzerotti, 2001; Lakhina and Tsurutani, 2016). The effects of geomagnetic irregular disturbances are usually observed on the Earth when the solar wind high-energy particles penetrate the Earth's magnetic field, also known as the geomagnetic field, extending from Earth's interior to outside the atmosphere (Love, 2008; Reeve, 2015; Yamazaki and Maute, 2017). These geomag-

* Corresponding author.
E-mail addresses: linminmin.my@kmitl.ac.th (L.M.M. Myint), kukkai@nict.go.jp (K. Hozumi), susaito@mpat.go.jp (S. Saito), pornchai.su@kmitl.ac.th (P. Supnithi).

https://doi.org/10.1016/j.asr.2022.06.024
0273-1177/

netic disturbances can typically last from a few hours to days, and the fluctuations range from a few to hundreds of nano Tesla (nT) (Love, 2008). In the space weather community, the geomagnetic disturbances have been continuously monitored by assessing geomagnetic indices, for example, the K-index, Kp-index, Dst (disturbance storm time) and auroral electrojet (AE) (Bartels, 1949; Du et al., 2010; Matzka et al., 2021). The K-index is an indicator of the intensity of the geomagnetic disturbances for many decades (Bartels et al., 1939; Menvielle et al., 1995). It is a quasi-logarithmic scale index, in the range of 0–9, derived from the maximum variations of the geomagnetic field data measured by a ground-based magnetometer. To monitor geomagnetic storms on a planetary scale, Bartels (1949) also introduced a Planetary K-index (Kp-index), which is the average standardized index derived from the K-indices of a global network of 13 geomagnetic observatories. Even though the Kp-index has been widely used as a critical indicator for global space weather monitoring, the network of observatories does not uniformly cover all continents or low latitude regions, and it does not provide information on small-scale disturbances (Stankov et al., 2011; Yi and Kim, 2018). Moreover, the local disturbances depend on the ionospheric current system and local times. Therefore, the local K-index from an individual geomagnetic station has become a key proxy for local disturbance monitoring and prediction (Hwang et al., 2013; Stankov et al., 2011; Valach et al., 2016).

Recently, numerous space weather centers have started to generate local K-indices using data from locally installed magnetometers for local or regional space weather forecasting (Corona-Romero et al., 2017; Denardini et al., 2015; Hwang et al., 2013) and disaster prevention (Stankov et al., 2011). The K-index is calculated from the maximum fluctuation of the horizontal components of the magnetic field, within every UT three-hour interval, after subtracting the Solar regular variation (S_R) curve, that represents daily regular geomagnetic variation (Bartels et al., 1939). The International Association of Geomagnetism and Aeronomy (IAGA) has adopted four computer-based K-index generating algorithms that can be used in any geomagnetic observatory around the world, without significant discrepancy (Hopgood, 1986; Menvielle et al., 1995): these algorithms use different S_R curve estimation techniques. Among them, the Finnish Meteorological Institute (FMI) or Finnish method proposed by Sucksdorff et al. (1991) provides the most acceptable results compared to the hand-scaling process, according to Menvielle et al. (1995), thus, it is widely used for K-index generation at many observatories (Bernard et al., 2012; Nevanlinna, 1999) and as a baseline method to evaluate other methods, for example, the nowcast method in space weather (Jian-Jun et al., 2017; Regi et al., 2020; Stankov et al., 2011). The FMI method employs a linear elimination method on the magnetic field data from three consecutive days to estimate the S_R curve of one day.

After the S_R curve is estimated and removed from the measured magnetic field in K-index computation, the maximum fluctuation of the residual field (K-variation) within a three-hour interval is converted into the respective K-index value using a table of the geomagnetic range lower limits for K-indices (a conversion table between the geomagnetic range scales and K-indices) of the observatory. Each observatory needs to develop its own table based on the characterization of the geomagnetic variations because the regular variation normally increases from the magnetic equator towards the aurora zone in each hemisphere (Bartels et al., 1939; Love, 2008). Therefore, the lower limits in the table for any specific observatory or station are calculated proportional to those in the table from the Niemegk Observatory, Germany (geographic coordinates: 52.07°N, 12.68°E, magnetic latitude (MLAT): 47.82°N) as a reference, after the lower limit K9 (L9) is determined (Bartels et al., 1939). Conventionally, a provisional value of L9 was initially assigned by the International Service of Geomagnetic Indices (ISGI), based on the observatory's magnetic latitude, but it can be calibrated by the statistical analysis of the geomagnetic indices at the given observatory and a historically recognized observatory (Regi et al., 2020). These statistical analysis methods were also used in validating the local K-indices from new local magnetometer stations (Corona-Romero et al., 2017; Hwang et al., 2013; Yi and Kim, 2018). Typically, the low L9 values were assigned to the stations at the low latitudes, but the stations at the magnetic equator need higher L9 values due to the local ionospheric current systems (Bartels et al., 1939). In Denardini et al. (2015), the L9 values for the low latitude regions were obtained by applying a least-squares polynomial fit equation, that was derived from the table of the latitudes and the L9 values of the existing stations.

In the magnetic equatorial region, it is well-known that the geomagnetic field variation during the daytime is dominated by the equatorial electrojet (EEJ) (Jose et al., 2011; Uemoto et al., (2010)). The EEJ is a strong eastward ionospheric current flowing along the magnetic equator in the E-layer of the ionosphere on the dayside. The cause of this strong zonal current is the effective zonal ionospheric conductivity, Cowling conductivity. During the daytime, in the vicinity of the magnetic equator, the high enhanced amplitudes of the horizontal components due to the EEJ current are observed in the geomagnetic field data measured (Abdul Hamid et al., 2013). The longitudinal and seasonal characteristics of EEJ have been intensively studied using the longitudinal and historical geomagnetic data (Abdul Hamid et al., 2014; Doumouya et al., 1998; Ismail et al., 2017; Yamazaki and Maute, 2017). According to Abdul Hamid et al. (2014), the day-to-day variability in the daily solar quiet (Sq) current and the EEJ current is mainly uncorrelated, and the characteristics of EEJ in the Southeast Asian sector differ from those in other regions, e.g., the Indian and South American. In Xiong et al. (2016),

the solar wind effects on the EEJ, the vertical plasma drift, and the thermospheric zonal wind were investigated based on observations from the satellites, and the study also showed that EEJ patterns depended on longitude.

Conventionally, the variations in magnetic field measurements, caused by EEJ, are considered non-K variations, which are a part of the SR curve. However, the day-to-day variation of the EEJ amplitudes is unpredictable, highly inconsistent, and longitudinally dependent; as a result, it is challenging to determine the L9 value and estimate the S_R curve in generating the local K-index. Moreover, it is worth investigating whether this is representative of the local K-index generated from the equatorial geomagnetic field under the influences of the various EEJ variations and how to alleviate the EEJ's regular variation in the equatorial K-index. Considering that the irregular variation of the geomagnetic fields in the equatorial region reflects the disturbances from the solar winds and various local features, this local K-index can help to predict local ionospheric irregularities and estimate ionospheric delays or total electron content (TEC).

Therefore, this work aims two objectives: (1) to generate local K-index from the equatorial magnetic field measured at Phuket geomagnetic station using a proper L9 value for local space weather monitoring and (2) to investigate the effects of EEJ on the local K-index. The Phuket's fluxgate magnetometer was installed at Phuket, Thailand as part of the Southeast Asia Low-latitude Ionospheric Network (SEALION) (Maruyama et al., 2007) under the National Institute of Information and Communications Technology (NICT), Japan. The location of the Phuket geomagnetic station (geographic coordinates: 8.100°N, 98.300°E, MLAT: 1.070°N) and local time (LT) = universal time (UT) + 7) is described in Fig. 1. The magnetic latitude was calculated using the IGRF-13 model with an epoch time of 2020.5. The magnetometer generates the raw geomagnetic fields data with a resolution of 0.01 nT and

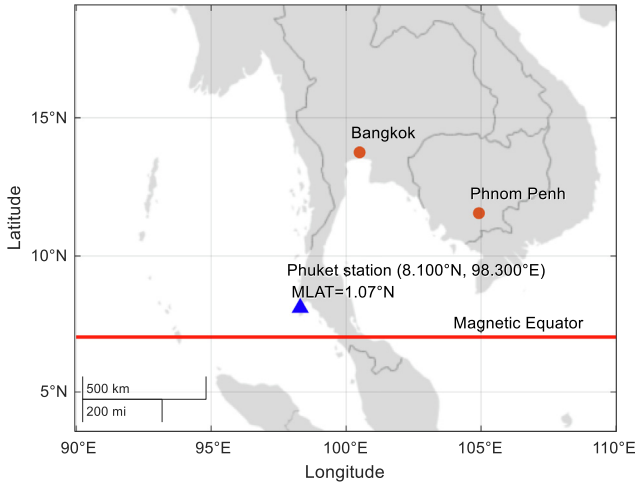

Fig. 1. Location of Phuket geomagnetic station (blue triangle) in Thailand. The magnetic equator is shown with a red line. [MLAT is computed by the IGRF-13 model].

1 Hz sampling rate. In this work, we computed the local K-indices using the conventional FMI method using the geomagnetic fields data with one-minute resolution measured from 2014 to 2019. The effects of EEJ on the estimated local K-indices were investigated, and appropriate L9 values were determined using statistical analysis with the values of the correlation coefficients and the root mean squared errors (RMSE) against the Kp-index. The monthly mean and the standard deviation as well as the diurnal variations of the magnetic field measurements in 2015 (high solar activity year) and 2019 (low solar activity year) were also examined.

2. Methodology

In the space weather monitoring community, the K-index is a quasi-logarithmic scale index, ranging from 0 to 9, derived from the variations of the geomagnetic field data measured from the ground-based magnetometer. There are two components of variations of the geomagnetic field measured from the ground magnetometer: long-term (secular) and short-term variations. The long-term variation is mainly related to the Earth's interior. On the other hand, short-term variation is mainly caused by solar activity: it can be further classified into daily regular variation and irregular variations (Reeve, 2015; Love, 2008). The daily regular variation or non-K-variation caused by the ionospheric current systems depending on the solar (local) time is also known as the daily solar regular (S_R) variation (Yamazaki and Maute, 2017). The causes of short-time irregular variations or K-variation are due to the powerful solar activities, e.g., solar flares, coronal mass ejections, high-speed solar wind and solar energetic particles. These types of variation include geomagnetic pulsations, magnetospheric substorms, geomagnetic storms, and other disturbances from rapid changes in the currents and fields in the magnetosphere (Matzka et al., 2021).

In K-index calculation, one of the most challenging tasks is systematic classification and removal of the non-K variation (or S_R curve) from the observed geomagnetic fields (Hopgood, 1986). Still, there is no straightforward guideline for estimation of the S_R curve for computer-based K-index derivation. Several computer-based S_R curve estimation methods were proposed and examined against the hand-scaling process by IAGA. The S_R curve can be estimated numerically by smoothing out the high frequency variations from a set of hourly mean values (HMV), based on daily data with adaptable window sizes (Hopgood, 1986; Sucksdorff et al., 1991; Nowozyński et al., 1991) or derived from the field data of the neighboring quiet days within a 27-day solar cycle (Takahashi et al., 2001; Stankov et al., 2011).

To generate the local K-index, we used the FMI method from Sucksdorff et al. (1991), because the derived K-indices are comparable to those generated by hand-scaling (Menvielle et al., 1995). In this method, the K-indices in any given day are computed from available three consecu-

tive days of geomagnetic field data with one-minute or better resolution (Stankov et al., 2011). Firstly, the 24 values of UT hourly mean value (HMV) for each horizontal component for one day are calculated with the three-day data (the previous day, the day itself and the next day). The MHV of the k^{th} hour is computed by averaging the 60 min data of magnetic field within that hour, plus (m_k +- n_k) minutes more on both sides of that hour. For example, the HMV of the geomagnetic field X component at the k^{th} hour is calculated as,

$$\bar{X}_k = \frac{1}{N}\sum_{i=-\tau_k}^{\tau_k} X_i, \text{ where } k \in \{0, 1, \ldots, 23\} \quad (1)$$

where X_i is the X component of the magnetic field data measured at minute i, N is the number of the one-minute field data points or the window size, and $\tau_k = 30 + m_k + n_k$ is the number of the minutes on each side of that hour k. Here, m_k is considered based on a three-hour interval in LT (i.e., 0 during the day, 60 min during dawn from 3 to 6 LT and dusk from 18 to 21 LT, and 120 min during nighttime from 21 to 3 LT) and n_k depends on the geomagnetic activity at hour k ($n_k = K^{3.3}$), where K values are the preliminary K-values or the K-index values from the previous step. After that, the S_R curve of the X component is estimated by fitting a 5th-degree harmonic to the HMV of each k. Similarly, the S_R curve for the Y component is also estimated simultaneously. The whole K-index calculation using the FMI method (Sucksdorff et al., 1991) is:

1. Determine the eight preliminary K-values of two horizontal components from the difference between the maximum and minimum of the respective field component at every three UT hours interval according to the table of the field range limit.
2. Compute the HMV of each component for the whole day from the geomagnetic fields of three consecutive days using Eq. (1).
3. Calculate the S_R curve of each component by fitting a 5th-degree harmonic to the HMV of the respective component.
4. Obtain the K-variation or the residual field of each component by subtracting the respective S_R curve from each component to remove the solar regular variation.
5. Determine the K-index for every 3-h interval from the difference between the maximum and minimum of the residual field from step 4.
6. Repeat steps 2 to 5 twice before generating the final K-indices for the target day.

In the FMI method, the conversion from the geomagnetic field range to a specific K-index value needs to be performed three times: two S_R curve estimation steps and the final K-index calculation step. At each time, the maximum fluctuation range of the geomagnetic field components is converted to its respective K-index according to the table of the limits of the geomagnetic field range classes. The range limits table for each observatory or station can be developed proportionally to the range limits of a reference Niemegk observatory with the L9 value from the target station. The field range lower limit, L_i, of the i^{th} K-index class for a station is.

$$L_i = L_9 \times \frac{L_i^{NGK}}{L_9^{NGK}}, \text{ where } i \in \{0, 1, ..., 9\} \quad (2)$$

where L_9 is the L9 value of the station, and L_i^{NGK} is the lower limit for the i^{th} K-index from the Niemegk observatory. It is worth mentioning the ISGI typically provides the initial L9 value for any geomagnetic station. Regi et al. (2020) calibrated the L9 values for two Italian stations by correlation analysis between the K indices for various L9 values from the observatories in the mid-latitude region and the closest historical observatory as a reference. The L9 values usually increase from low latitudes to the aurora zone in each hemisphere (Love, 2008); however, the values at the equatorial station needs to be higher than in the low latitude region because of the EEJ effects (Mayaud, 1980). Denardini et al. (2015) calculated L9 values of the magnetometer stations in the South American, including the equatorial region, from a least-squares polynomial fit of the plot of the relationship between the geomagnetic latitudes (λ) and the L9 values of the existing magnetic observatories, i.e.,

$$L9(\lambda) = 0.48\lambda^2 - 23.79\lambda + 572.04. \quad (3)$$

Therefore, the L9 value for any magnetometer station can be roughly calculated using (3). However, according to Abdul Hamid et al. (2014) and Yamazaki and Maute, (2017), day-to-day variations of EEJ are inconsistent and unpredictable in longitudinally different regions, thus the suitable L9 value for the equatorial station needs to be determined carefully. Moreover, it can alleviate the EEJ effect and not fail to detect the geomagnetic disturbances. Therefore, following Hwang et al. (2013) and Regi et al. (2020), we examined the correlation coefficients between the local K-indices with various L9 values and the Kp-indices to obtain the proper L9 value for the magnetometer station at Phuket. The Pearson correlation coefficient, r, between the values of the local K-index from Phuket station and the Kp-index over many years was calculated from,

$$r = \frac{\sum_{i=1}^{N}\left(K_i - \bar{K}\right)\left(Kp_i - \bar{K}\,p\right)}{\sqrt{\sum_{i=1}^{N}\left(K_i - \bar{K}\right)^2 \sum_{i=1}^{N}\left(Kp_i - \bar{K}\,p\right)^2}}, \quad (4)$$

where N is the total number of data points, K_i and Kp_i are the values of local K-index and Kp-index at time i, and $\bar{K}$ and $\bar{K}p$ are the averages of the indices. Moreover, we investigated the root mean square error, RMSE, between the local K-indices with different L9 values and Kp-indices over long periods computed as,

$$RMSE = \sqrt{\frac{\sum_{i=1}^{N} (K_i - Kp_i)^2}{N}}. \quad (5)$$

Finally, the distributions of the local K-indices generated with the appropriate L9 values compared to the Kp-indices were analyzed.

3. Analysis of geomagnetic fields at equatorial Phuket station

We first investigated equatorial geomagnetic field data with one-minute resolution from the fluxgate magnetometer installed at Phuket geomagnetic station under SEALION project by NICT, Japan. We examined two components, X and Y, of the magnetic fields in this study even though component Y's variation was considerably lower than that of component X in the low latitude region. Since we wanted to focus on the short-term geomagnetic variation, the secular variation was removed from each component of the original magnetic field data by subtracting the daily medians of the respective component following (Stankov et al., 2011). The X and Y components of the magnetic field, after removing the secular variation, are denoted by the *relative geomagnetic fields*, ΔX and ΔY. This section examined the monthly mean and diurnal variations of the equatorial geomagnetic fields based on data collected in 2015 (high solar activity) and 2019 (low solar activity). Moreover, the diurnal variation of geomagnetic fields in the equinoctial month (March) and a solstitial month (June) of 2015 and 2019 were studied against the Ap-index, a daily index of planetary geomagnetic activity to investigate EEJ variations.

3.1. Monthly variation of the geomagnetic field

The monthly averages of the relative geomagnetic components, ΔX and ΔY, in each month of 2015 and 2019 were investigated to observe the trend of the magnetic equatorial geomagnetic field under the influence of EEJ effects. Fig. 2 (a) and (b) show the monthly average ΔX and ΔY in 2015 (solid red line) and 2019 (blue dashed line) at each hour (LT = UT + 7). The shaded area around each curve represents the standard deviations from the mean and the local noon time (12 LT) is indicated by a dash dot line in each month. According to Fig. 2 (a), the monthly average of ΔX during daytime was relatively higher than during nighttime, due to the EEJ variations. The daytime peaks of ΔX in 2015 (high solar activity year) were noticeably higher than those in 2019 (low solar activity year), because the magnitude of EEJ was generally higher during solar maximum, due to increased ionization in the ionosphere, as explained by (Ismail et al., 2017). The ΔX field was much lower and close to zero during the night when the EEJ and Sq currents disappeared. Its day-to-day standard deviations in each month were also higher in 2015. The highest means and standard deviations of ΔX were observed in the March equinox 2015. In both years, the daytime peaks of ΔX in March, April, September, and October were higher than in other months, indicating the seasonal dependence. Yamazaki and Maute (2017) attributed this to the enhanced Sq amplitude, during equinoctial months at low and equatorial latitudes.

Fig. 2 (b), similarly, illustrates the monthly ΔY means in both years. There was no significant difference in the field variations between the two years, except that in February 2015, the highest daytime magnetic field ΔY was reached a few hours earlier than 2019. In addition, the changes in ΔY were significant and fast during daytime, but small and slow changes were found at night. The standard deviations in most of the months were similar except for the first three months. It is also worth noting that the trends of ΔY variations from May to September were similar, and the trends in January-March and November-December were also similar. However, the patterns of the ΔY variation in the equinoctial months, March and October, in both years were unique, and the ΔY field fluctuations in those two months were small, compared to those in other months; thus, the characteristics of ΔX and ΔY are contrary.

3.2. Diurnal variability of geomagnetic field

In Fig. 3, we compared the diurnal variations of the relative geomagnetic field X component, ΔX with the Ap-index in March and June of 2015 and 2019. The Ap-index of each day is printed inside the boxes at the bottom of the graph. The colors in the text of Ap-index and the field curve encode levels of planetary geomagnetic disturbances, i.e., black for 'no or low disturbance levels', yellow for the 'active disturbances' and red for the 'geomagnetic storm levels.' The Ap-indices were from the website of the Helmholtz Centre Potsdam-GFZ German Research Centre for Geosciences (https://www-app3.gfz-potsdam.de/kp_index/Kp_ap_Ap_SN_F107_since_1932.txt), and we also marked five international quietest days in each month with the data downloaded from (ftp://ftp.gfz-potsdam.de/pub/home/obs/kp-ap/quietdst/). The horizontal axis indicates the day of year (DoY).

Fig. 3 (a) and (b) show that the daily peaks of ΔX due to EEJ in the daytime in general varied between 100 nT and 240 nT in March 2015, and between 80 nT and 150 nT in June 2015. The peaks in these two months were mostly ~ 150 nT for March and 100 nT for June. However, on some days, large Ap-indices (affected by the geomagnetic storms) were evident, particularly eight DoYs 60, 61, 76, 77, 78, 79, 81, and 82 in March 2015, and four DoYs 159, 173, 174 and 176, in June 2015. Extreme distorted short-term geomagnetic variations were identified on two consecutive days on two occasions, DoYs 76 and 77, and 173 and 174. During the two-day storms, the fluctuations of the magnetic fields on the first day were signif-

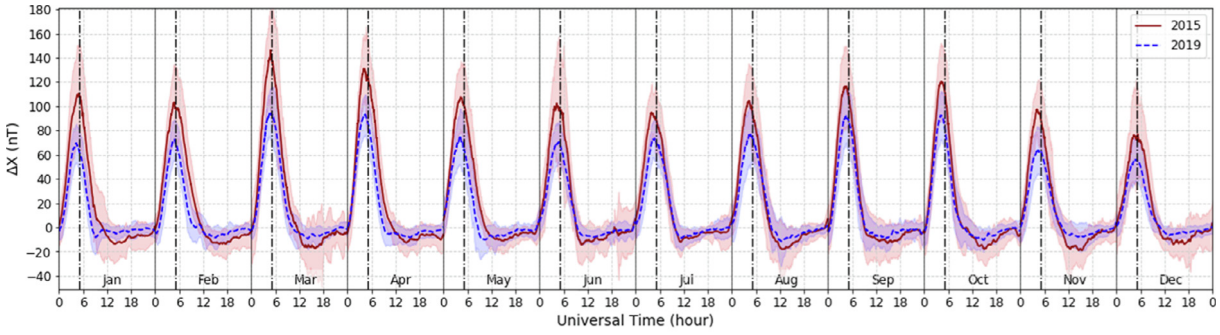

(a) ΔX

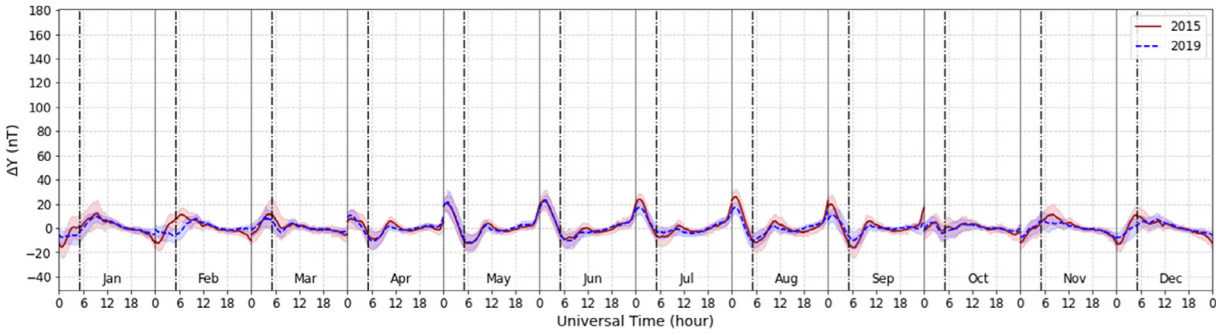

(b) ΔY

Fig. 2. Monthly means of the relative geomagnetic field components (solid line) and the standard deviations from the mean (shaded area): (a) ΔX and (b) ΔY in 2015 and 2019 [the vertical dash dot lines represent noon 12 LT].

icantly higher than on other normal days, but the EEJ amplitude during the daytime was depressed on the second day. The reduction in the geomagnetic fields was due to a developing westward ring current in the magnetosphere (Yamazaki and Maute, 2017). In general, the nighttime ΔX variations varied every day, and short-duration fluctuations were often detected in both months of the high solar activity year. On the disturbed days, ΔX values dropped significantly at night. The frequent instances of counter electrojet (CEJ) or reversed flow of the equatorial electrojet were also seen in both months, significantly in DoYs 70, 72, 81, 165–168. Among the five quietest days, the patterns of ΔX during the daytime were similar, with different EEJ peaks, and were rather flat during the night, except on DoY 64. Yamazaki and Maute (2017) suggested that neutral winds were the reason for the day-to-day variability due to Sq and EEJ for days without solar and geomagnetic activity.

Fig. 3 (c) and (d) show peaks of ΔX were lower for each day in 2019 (low solar activity year) than in 2015. The planetary geomagnetic activity was primarily low except for a few days. The peaks of the variations ranged from 60 nT to 150 nT in the equinoctial month, March, and between 50 nT and 100 nT in the solstitial month, June. In 2019, rapid ΔX fluctuations during the night were also observed on the day with high Ap-indices, where the EEJ variation during the daytime were superimposed on them, so they were not observable. The ΔX variations on quiet days were very similar except on DoY 77 in March when the daytime ΔX peak was relatively low compared to other quiet days, attributed to high geomagnetic activity on the previous days. Even though the values of the Ap-index are not as high as in 2015, a few active geomagnetic disturbances with the Ap-index above 10 occurred in March, but they were rare in June.

Based on the Ap-index values, the above analyses show that the geomagnetic field ΔX variations were consistent with the planetary geomagnetic activity levels. During the daytime, the effects of the EEJ current mostly dominated the geomagnetic variation. Consequently, different characteristics of the equatorial geomagnetic field were perceived during daytime and night independently. The daily variances of the EEJ amplitudes were high and unpredictable, even on quiet days; as a result, it was challenging to determine the L9 value and estimate the S_R curve at a geomagnetic station in the equatorial region. During the night, the fields were generally stable for quiet days. When the geomagnetic activity was high, irregular variations were detected during both daytime and night. The variability of the daytime field amplitudes from day-to-day was relatively high in 2015 (high solar activity) but moderate in 2019 (low solar activity).

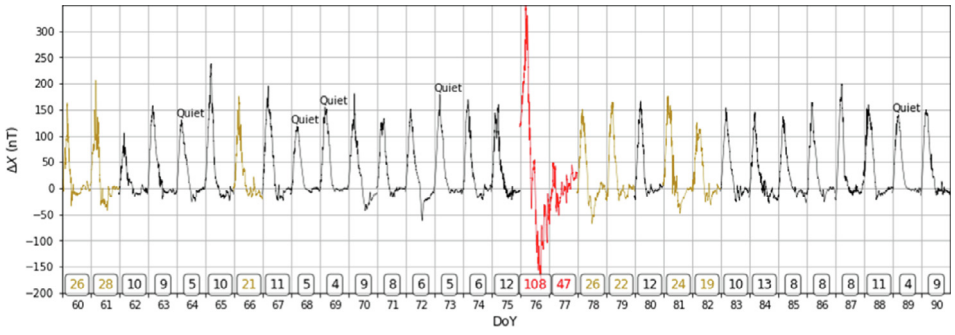

(a) March 2015

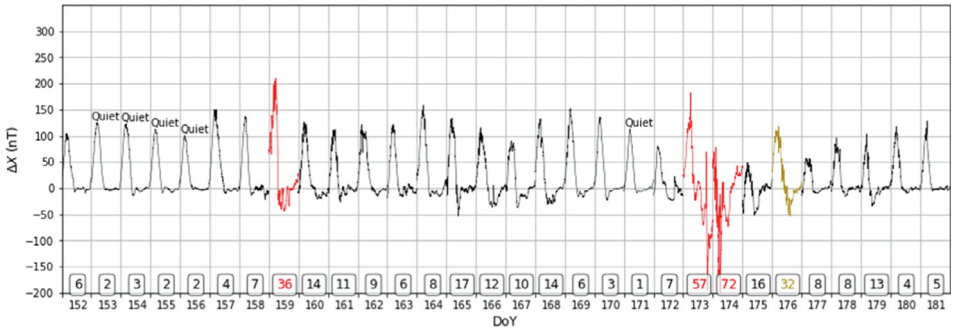

(b) June 2015

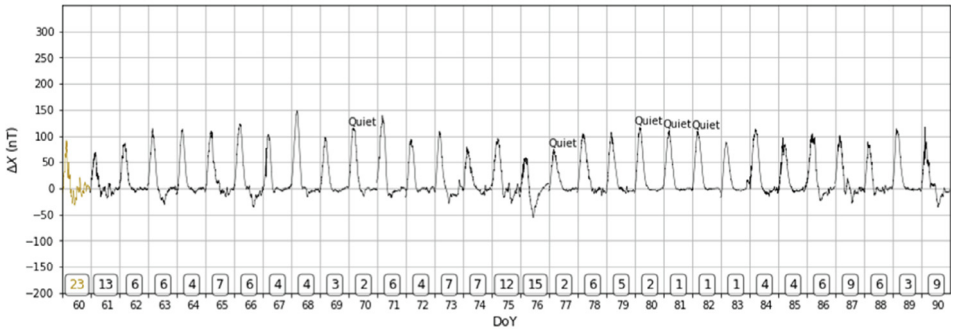

(c) March 2019

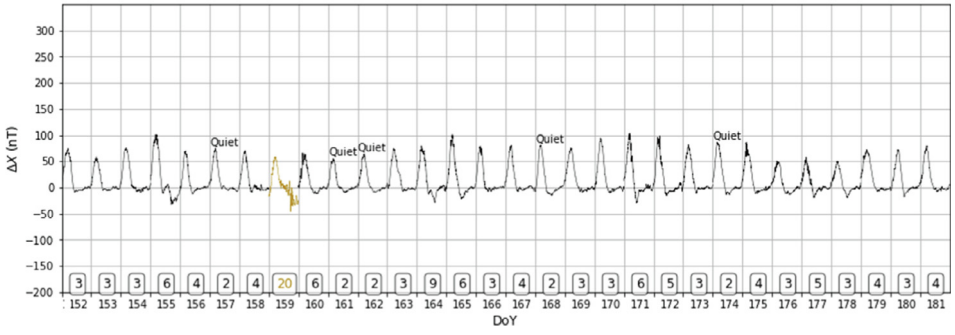

(d) June 2019

Fig. 3. Diurnal variations of ΔX components versus daily Ap index in March and June of 2015 and 2019. [black for 'no or low disturbance levels', yellow for the 'active disturbances' and red for the 'geomagnetic storm levels' based on Ap index].

4. Local K-index generation from Phuket magnetometer station

4.1. L9 value for Phuket magnetometer station

To estimate the local K-index from the magnetic field data, the proper L9 value needs to be determined first, because it depends on the station's geomagnetic latitude as well as the impacts of local features. As the EEJ impacts the local K-index in the equatorial region, the equatorial station's L9 value was higher than that for mid-latitude stations (Bartels et al., 1939). According to Eq. (3) from (Denardini et al., 2015), the L9 value for the Phuket's magnetic latitude was calculated to 547 nT. Since the characteristics of EEJ also differ longitudinally, this L9 still needs to be adjusted based on the statistical analyses. Hwang et al. (2013) and Regi et al. (2020) studied the local K-indices with various L9 values statistically, by comparing with the global geomagnetic index or Kp-index values (as a reference index) to find a proper L9 value. For this purpose, we computed local K-indices from Phuket equatorial geomagnetic field data for 1667 days measured from 2014 to 2019 with the FMI method, where the L9 value was used in both S_R curve estimation and K-index calculation; hence we used the L9 value as a control parameter to alleviate the prominent effect of the daily EEJ variation in the local K-index computed from the equatorial region. Then, to obtain a suitable L9 value, we used statistics from local K-indices computed with different L9 values and the Kp-indices.

Firstly, the correlation coefficients, r, between the K-indices at Phuket station and the Kp-indices using Eq. (4) were plotted as a function of L9 values as shown in Fig. 4. To observe the effects of EEJ on the K-index, we examined the three correlation coefficients between the two indices for (a) the whole day (0–24-hour UT or 7–next day's 7-hour LT), (b) during daytime (0–12-hour UT or 7–19-hour LT) and (c) nighttime (12–24-hour UT or 19–next day's 7-hour LT). Of all L9 values, Phuket's K-indices during the night were better correlated to the Kp-indices than the daytime ones, due to the lack of local EEJ at night. The correlations from the nighttime were similar for all L9 values, especially from 300 nT to 700 nT. It is important to note that the proportion of high Kp-index values in the dataset was considerably less than the proportion of low index values, because the geomagnetic activity usually is low, and severe disturbances were rare. As a result, we observed that the correlations between two indices for both the whole day and night periods increased with L9. K-index calculations with high L9 values produced fewer high K-indices than low L9 values, so the local K-index dataset generated with the higher L9 values was closer to the Kp-index dataset. However, we need to be aware that a high L9 value can lead to inaccurate classification of severity of geomagnetic disturbances and local disturbances.

Since the cross correlation does not provide a definitive L9 value, we computed root mean square errors (RMSE) between Phuket local K-indices with various L9 values and Kp-indices (from 2014 to 2019) using Eq. (5). The plots of RMSE from the whole day, daytime and nighttime are shown in Fig. 5. The errors from the daytime data dropped rapidly with increasing L9 and then do not change noticeably for L9 > 650. However, the errors during nighttime reached a minimum at 400 nT, and after that, became worse with higher L9 values. Due to the different error behaviors between the day and night data, a minimum error for the whole day data was found at 600 nT. Since the minimum RMSE values were achieved at 400 nT for nighttime and 600 nT for daytime and the wholeday respectively, we considered the L9 values from 400 nT to 600 nT with a step size of 100 nT for further study. We did not consider the L9 > 600 nT, even though the daytime error further decreased, because a higher L9 might fail to detect severe solar disturbances, particularly during the night. Similarly, we did not consider the L9 < 400 nT because of rapidly increment in errors for the K-indices in the whole day and the daytime.

4.2. Results and discussions

In the literature, the difference between two K-indices (or the K-index and Kp index), ΔK, was usually used to

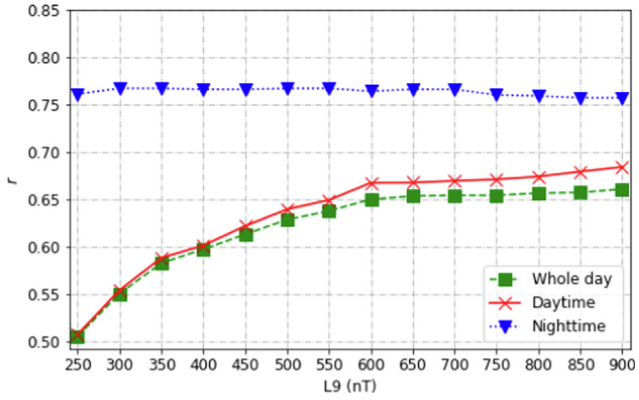

Fig. 4. Correlation coefficients, r, between values of local K-indices from Phuket and Kp-indices versus L9 (x-axis) from 2014 to 2019.

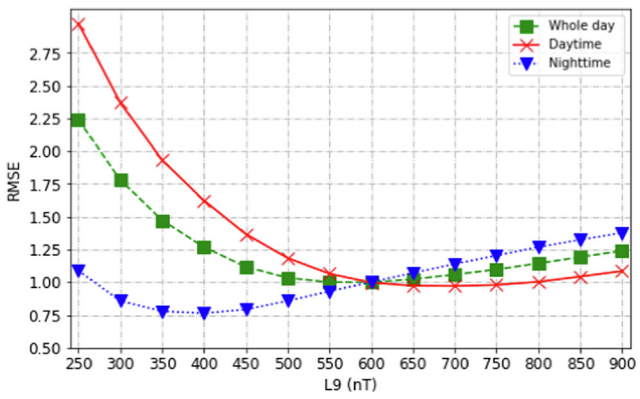

Fig. 5. Root mean square errors (RMSEs) between the local K-indices from Phuket and Kp-indices versus L9 (x-axis) from 2014 to 2019.

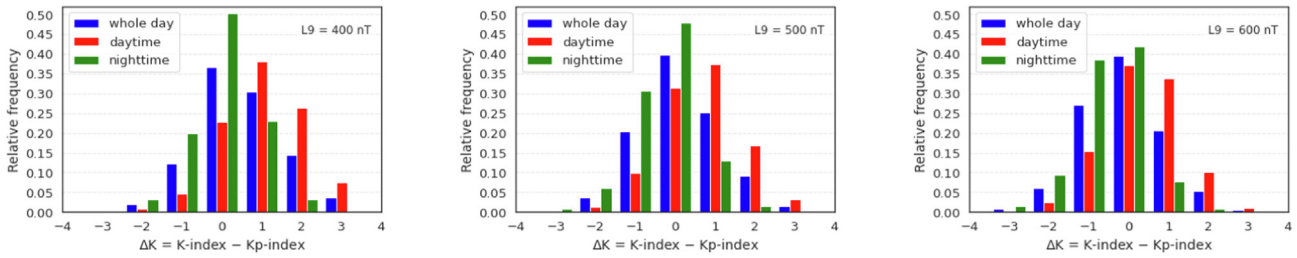

Fig. 6. Distributions of ΔK = (Phuket's local K-index - Kp-index) with three L9 values: (a) 400 nT, (b) 500 nT, and (c) 600 nT for the whole day, daytime and nighttime.

validate the K-index from a new station or a new method (Menvielle et al., 1995; Nowozyński et al., 1991; Sucksdorff et al., 1991; ; Stankov et al., 2011; Regi et al., 2020). If the local K-index from the target station agreed with the reference K-index (or the Kp-index), the differences between the two K-indices were minor. In this study, we analyzed the relative frequency distributions of ΔK, which is the difference between the time series data (from 2014 to 2019) of the Phuket local K-indices computed with three L9 values – 400 nT, 500 nT and 600 nT -and the Kp index as described in Fig. 6. To observe the EEJ influence, ΔK values for the whole day, day and night times were computed and plotted. Since the Kp-index is indicated in 28 classes for separated by thirds of a unit, and labelled as x-, x and x+, for example 6- is 5 2/3, 6 is 6 and 6+ is 6 1/3, we adjusted all Kp-index values, by rounding to the nearest integer to be at the same scale levels as the K-index. Histograms of values of ΔK with the L9 = 400 nT from the whole day, day and night times, are plotted together in Fig. 6 (a). The proportion of ΔK = 0 on the entire day was over 35 %, but most of Phuket's local K-indices (about 50%) were still higher the Kp–indices. The distribution of ΔK for the daytime data was symmetric about ΔK = 1, implying that the local K-index during daytime was mostly higher than the Kp-index. In contrast, ~50% of the K-indices during nighttime matched the Kp–indices.

When the L9 value was increased to 500 nT in Fig. 6 (b), 40% of the ΔK distribution from the whole day was seen at ΔK = 0 and the proportion of both ± 1 index errors was more than 45%. However, the local K-indices during the daytime were still higher than Kp-indices as the highest proportion of the daytime data was seen at ΔK = 1. Compared to the low L9 value, its proportion of ΔK = 0 was higher. On the other hand, the highest distribution of the nighttime data was still at ΔK = 0, but the second largest (30%) was at ΔK = -1. When the ΔK values with L9 = 600 nT were examined in Fig. 6 (c), the highest distributions of all three data were obtained at ΔK = 0. The proportion of the negative ΔK from the whole day was 33% and for nighttime 50%, implying that the local K-index underestimated some significant solar nighttime disturbances. In contrast, K-indices from the daytime seemed to be slightly better than other lower L9 values.

These results showed that L9 values of 500 nT and 600 nT were acceptable for the local K-index calculation with Phuket magnetic data because about 40% of K-indices for the whole day matched Kp-indices, even though the local K-indices during the daytime were higher than the Kp-indices because of the effects of EEJ and other local features. Therefore, the different characteristics of the diurnal geomagnetic variations between the daytime and the nighttime at the equator region made it challenging to determine a suitable L9 for the Phuket station.

We also examined the distribution of K-indices compared to Kp-indices on the entire day from 2014 to 2019 for the L9 values – 400 nT, 500 nT, and 600 nT – in Fig. 7. High discrepancies between the local K-indices and the Kp-indices were found, particularly at low index values from 0 to 3 at L9 = 400 nT, as illustrated in Fig. 7 (a). These discrepancies at the low index values became smaller at L9 = 500 nT as seen in Fig. 7 (b); how-

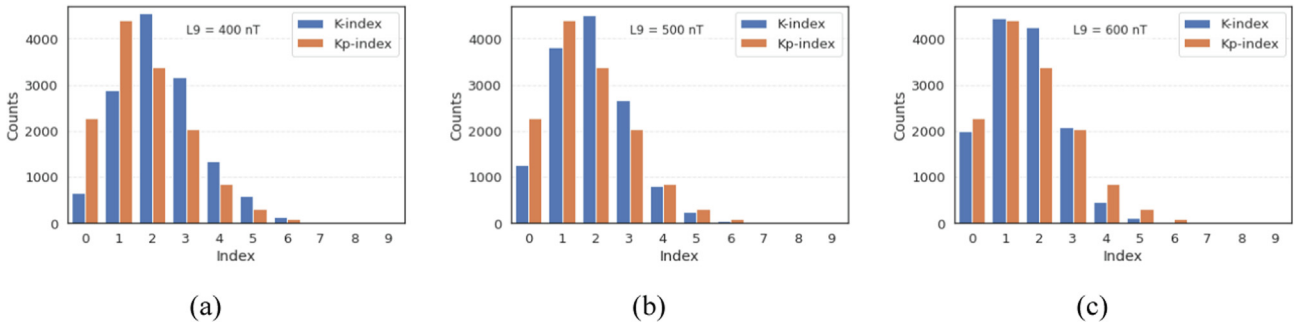

Fig. 7. Distributions of Phuket local K-indices against Kp-indices for the whole day for L9 values: (a) 400 nT, (b) 500 nT, and (c) 600 nT.

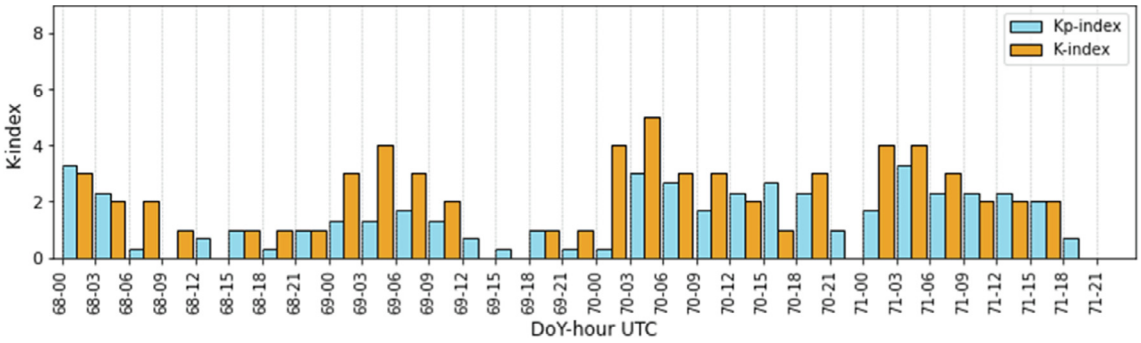

(a) March 2015

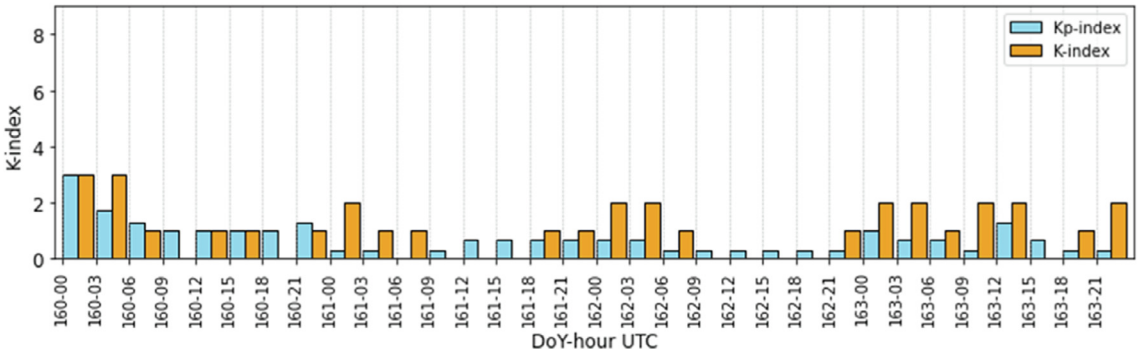

(b) June 2019

Fig. 8. Phuket's local K-index computed with L9 = 500 nT and Kp-index in vs time (UTC) fro (a) March 2015 (high solar activity) and (b) June 2019 (low solar activity).

ever, occurrences of high local K-indices, i.e., 4, 5 and 6, were slightly less than those of the Kp-index. According to Fig. 7 (c), the local K-index mostly failed to indicate accurately the high and severe geomagnetic storms at L9 = 600 nT. Therefore, these results confirmed again that 500 nT was suitable for the L9 value used in the local K-index calculation with the geomagnetic field measured from the equatorial Phuket station.

In addition, we compared Phuket's local K-index computed with L9 = 500 nT and Kp-index for March 2015 (high solar activity) and June 2019 (low solar activity), as shown in Fig. 8. In both months, the values of the two indices were generally close. However, in the daytime period of March 2015 in Fig. 8 (a), local K-indices were slightly higher than Kp-indices due to the active EEJ variation on those days, see Fig. 3 (a). Fig. 8 (b) shows that the discrepancy between the two indices was less in June 2019. Therefore, the effects of EEJ on local the K-indices can be partially controlled by considering an appropriate L9 value. We expect these local K-index values to be helpful for local space weather study and disturbance assessment.

5. Conclusion

This study first investigated the geomagnetic field components ΔX and ΔY measured by the equatorial Phuket magnetometer station in 2015 (high solar activity year) and 2019 (low solar activity year). As expected, the variation of the ΔX component in the daytime was dominated by the EEJ current besides the Sq current. From the monthly mean variation study, seasonal variations of the geomagnetic field components were observed. The contrary features of those two field components were also seen in March and October. The inconsistent day-to-day changes of the EEJ variations, even on the quietest day, were observed from studying the diurnal variations. It is well known that the characteristics of EEJ vary longitudinally and seasonally (Ismail et al., 2017; Venkatesh et al., 2015). However, the geomagnetic field variations, ΔX, at Phuket were mostly consistent with the planetary geomagnetic activity level.

Due to the highly inconsistent day-to-day changes of EEJ, local K-index computation is a challenging task for an equatorial geomagnetic station to achieve high accuracy classification of geomagnetic disturbances. Therefore, we investigated the effect of EEJ on the local K-indices computed by the FMI method with the geomagnetic field data measured at the Phuket magnetometer for various L9 values. We found that the daytime EEJ degraded the performance of the K-index calculation, when the L9 value was set too low or high. After analyzing the distributions of Phuket local K-indices and the Kp-indices, the EEJ effect can be partially controlled in the local K-index calculation, if the L9 value was set appropriately. From the results, the

L9 value of 500 nT could produce the K-indices, classifying the geomagnetic disturbances more accurately. Since Phuket's local K-index represents local features, for example EEJ, it can be applied to the local ionospheric disturbance prediction model that is helpful for satellite communication and navigation applications. Therefore, we will further analyze the local K-index with other local space weather parameters, for example the critical frequency of ionospheric F2 lay (foF2), the F layer height (h'F), the F2-layer peak electron density (NmF2), TEC, etc.

Declaration of Competing Interest

The authors declare that they have no known competing financial interests or personal relationships that could have appeared to influence the work reported in this paper.

Acknowledgement

This work was partially funded by the NSRF via the Program Management Unit for Human Resources & Institutional Development, Research and Innovation [grant number B05F640197] and King Mongkut's Institute of Technology Ladkrabang [grant no. RE-KRIS/FF65/35]. The ASEAN IVO (http://www.nict.go.jp/en/asean_ivo/index.html) project, [GNSS and Ionospheric Data Products for Disaster Prevention and Aviation in Magnetic Low- Latitude Regions (Phase II)], was also involved in the production of the contents of this work and financially supported by NICT (http://www.nict.go.jp/en/index.html). Kornyanat Hozumi was partially supported by JSPS KAKENHI Grant Number 20H00197.

References

Abdul Hamid, N.S., Liu, H., Uozumi, T., Yumoto, K., 2013. Equatorial electrojet dependence on solar activity in the Southeast Asia sector. Antarctic Record 57 (3), 329–337. https://doi.org/10.15094/00009708.

Abdul Hamid, N.S., Liu, H., Uozumi, T., et al., 2014. Relationship between the equatorial electrojet and global Sq currents at the dip equator region. Earth Planets Space 66 (146). https://doi.org/10.1186/s40623-014-0146-2.

Astafyeva, E., Yasyukevich, Y., Maksikov, A., Zhivetiev, I., 2014. Geomagnetic storms, super-storms, and their impacts on GPS-based navigation systems. Space Weather 12 (7), 508–525. https://doi.org/10.1002/2014SW001072.

Baker, D.N., Daly, E., Daglis, I., Kappenman, J.G., Panasyuk, M., 2004. Effects of space weather on technology infrastructure. Space Weather 2 (2). https://doi.org/10.1029/2003SW000044.

Bartels, J., 1949. The standardized index, Ks, and the planetary index. Kp. IATME Bull 97 (12b), 0001.

Bartels, J., Heck, N.H., Johnston, H.F., 1939. The three-hour-range index measuring geomagnetic activity. Terr. Magn. Atmos. Electr. 44 (4), 411–454. https://doi.org/10.1029/TE044i004p00411.

Bernard, A., Menvielle, M., Chambodut, A., 2012. On the influence of the data sampling interval on computer-derived k-indices. Data Sci. J. 10, 41–46. https://doi.org/10.2481/dsj.IAGA-07.

Corona-Romero, P., Sergeeva, M., Gonzalez-Esparza, J.A., et al., 2017. Kmex: the Mexican geomagnetic k index. Latinmag. Lett. 7 (Special Issue), 1–6. https://doi.org/10.29327/2pangeo.a29.

Denardini, C., Rockenbach, M., Gende, M., Chen, S., 2015. The initial steps for developing the South American K index from the EMBRACE magnetometer network. Rev. Bras. Geofísica 33 (1), 79–88. https://doi.org/10.22564/rbgf.v33i1.603.

Doumouya, V., Vassal, J., Cohen, Y., Fambitakoye, O., Menvielle, M., 1998. Equatorial electrojet at African longitudes: first results from magnetic measurements. Ann. Geophys. 16 (6), 658–676. https://doi.org/10.1007/s00585-998-0658-9.

Du, D., Zhao, M., Lu, J., Yang, G., 2010. A sensitive geomagnetic activity index for space weather operation. Space Weather 8 (12), S12006. https://doi.org/10.1029/2010SW000609.

Hopgood, P., 1986. On the computer generation of geomagnetic K-indices from digital data. J. Geomagn. Geoelec. 38 (9), 861–871. https://doi.org/10.5636/jgg.38.861.

Hwang, J., Kim, H.-P., Park, Y.-D., 2013. Comparison of K-index calculations between several geomagnetic stations during IQDs and IDDs. J. AstroN. Space Sci. 30 (3), 169–174. https://doi.org/10.5140/JASS.2013.30.3.169.

Ismail, W., Abdul Hamid, N.S., Abdullah, M., Yoshikawa, A., Uozumi, T., 2017. Longitudinal variation of EEJ current during different phases of solar cycle. J. Phys. Conf. Ser. 852 (1). https://doi.org/10.1088/1742-6596/852/1/012019 012019.

Jian-Jun, W., Qi, L., Dong-Mei, Y., Jing-Hui, L., 2017. An improved FMI method of deriving K indices. Chin. J. Geophys. 60 (7), 321–332. https://doi.org/10.1002/cjg2.30049.

Jose, L., Ravindran, S., Vineeth, C., Pant, T., 2011. Investigation of the response time of the equatorial ionosphere in context of the equatorial electrojet and equatorial ionization anomaly. Ann. Geophys. 29 (7), 1267–1275. https://doi.org/10.5194/angeo-29-1267-2011.

Xiong, C., Lühr, H., Fejer G, B., 2016. The response of equatorial electrojet, vertical plasma drift, and thermospheric zonal wind to enhanced solar wind input. Journal of Geophysical Research: Space Physics 121 (6), 5653–5663. https://doi.org/10.1002/2015JA022133.

Yamazaki, Y., Maute, A, 2017. Sq and EEJ—A Review on the Daily Variation of the Geomagnetic Field Caused by Ionospheric Dynamo Currents. Space Science Reviews 206 (1), 299–405. https://doi.org/10.1007/s11214-016-0282-z.

Yi, Wonhyeong, Kim, Jiyoung, 2018. Comparison of planetary and local geomagnetic disturbance indices: Operational implications. Journal of Atmospheric and Solar-Terrestrial Physics 178, 1–6. https://doi.org/10.1016/j.jastp.2018.04.016.

Lakhina, G.S., Tsurutani, B.T., 2016. Geomagnetic storms: historical perspective to modern view. Geosci. Lett. 3 (1), 5. https://doi.org/10.1186/s40562-016-0037-4.

Lanzerotti, L.J., 2001. Space weather effects on communications. In: Daglis, I.A. (Ed.), Space Storms and Space Weather Hazards. Springer, Dordrecht, https://doi.org /10.1007/978-94-010-0983-6_12.

Love, J.J., 2008. Magnetic monitoring of earth and space. Phys. Today 61 (2), 31–37. https://doi.org/10.1063/1.2883907.

Maruyama, T., Kawamura, M., Saito, S., et al., 2007. Low latitude ionosphere-thermosphere dynamics studies with ionosonde chain in Southeast Asia. Ann. Geophys. 25 (7), 1569–1577. https://doi.org/10.5194/angeo-25-1569-2007.

Matzka, J., Stolle, C., Yamazaki, Y., Bronkalla, O., Morschhauser, A., 2021. The geomagnetic Kp index and derived indices of geomagnetic activity. Space. Weather 19 (5). https://doi.org/10.1029/GM022, p. e2020SW002641.

Mayaud, P.N., 1980. Derivation, Meaning, and Use of Geomagnetic Indices. American Geophysical Union, Washington, D. C., doi:10.1029/2020SW002641.

Menvielle, M., Papitashvili, N., Häkkinen, L., Sucksdorff, C., 1995. Computer production of K indices: review and comparison of methods. Geophys. J. Int. 123 (3), 866–886. https://doi.org/10.1111/j.1365-246X.1995.tb06895.x.

Nevanlinna, H., 1999. Geomagnetic observations at Sodankylä during the first international polar year. Geophysica 35 (1–2), 15–22.

Nowozyński, K., Tomasz, E., Jankowski, J., 1991. Adaptive smoothing method for computer derivation of K-indices. Geophys. J. Int. 104 (1), 85–93. https://doi.org/10.1111/j.1365-246X.1991.tb02495.x.

Reeve, W. D., 2015. Geomagnetism tutorial. [Online] Available at: https://reeve.com/Documents/ SAM/Geomagnetism Tutorial.pdf.

Regi, M., Bagiacchi, P., Di Mauro, D., et al., 2020. On the validation of K-index values at Italian geomagnetic observatories. Geosci. Instrum. Methods Data Syst. 9 (1), 105–115. https://doi.org/10.5194/gi-9-105-2020.

Stankov, S., Stegen, K., Warnant, R., 2011. K-type geomagnetic index nowcast with data quality control. Ann. Geophys. 54 (3), 285–295.

Sucksdorff, C., Pirjola, R., Häkkinen, L., 1991. Computer production of K-indices based on linear elimination. Geophys. Trans. 36, 333–345.

Takahashi, K., Toth, B.A., Olson, J.V., 2001. An automated procedure for near-real-time Kp estimates. J. Geophys. Res. Space Phys. 106 (A10), 21017–21032. https://doi.org/10.1029/2000JA000218.

Uemoto, J., Maruyama, T., Saito, S., Ishii, M., Yoshimura, R., 2010. Relationships between pre-sunset electrojet strength, pre-reversal enhancement and equatorial spread-F onset. Annales Geophysicae 28 (2), 449–454. https://doi.org/10.5194/angeo-28-449-2010.

Valach, Fridrich, Hejda, Pavel, Revallo, Miloš, Bochníček, Josef, Váczyová, Magdaléna, 2016. Testing the interactive computer method (IM) for producing K indices with the data of the Hurbanovo and Budkov magnetic observatories. Journal of Atmospheric and Solar-Terrestrial Physics 147, 90–97. https://doi.org/10.1016/j.jastp.2016.07.010.

Venkatesh, K., Fagundes, P.R., Prasad, D.S.V.V.D., Denardini, C.M., de Abreu, A.J., de Jesus, R., Gende, M., 2015. Day-to-day variability of equatorial electrojet and its role on the day-to-day characteristics of the equatorial ionization anomaly over the Indian and Brazilian sectors. J. Geophys. Res. Space Physics 120 (10), 9117–9131. https://doi.org/10.1002/2015JA021307.